JOURNAL OF CHEMICAL INFORMATION AND MODELING

Article

pubs.acs.org/jcim

Mesoscopic Simulation of Phospholipid Membranes, Peptides, and Proteins with Molecular Fragment Dynamics

Andreas Truszkowski,*[,†,‡] Karina van den Broek,[⊥] Hubert Kuhn,[§,†] Achim Zielesny,[‡] and Matthias Epple[†]

[†]Inorganic Chemistry and Center for Nanointegration Duisburg−Essen (CENIDE), University of Duisburg−Essen, 45141 Essen, Germany

[‡]Institute for Bioinformatics and Cheminformatics, Westphalian University of Applied Sciences, 45665 Recklinghausen, Germany

[⊥]Department of Pharmacy−Center for Drug Research, Ludwig-Maximilians University Munich, 80539 Munich, Germany

[§]CAM-D Technologies, 45127 Essen, Germany

ABSTRACT: Molecular fragment dynamics (MFD) is a variant of dissipative particle dynamics (DPD), a coarse-grained mesoscopic simulation technique for isothermal complex fuids and soft matter systems with particles that are chosen to be adequate fluid elements. MFD choses its particles to be small molecules which may be connected by harmonic springs to represent larger molecular entities in order to maintain a comparatively accurate representation of covalent bonding and molecular characteristics. For this study the MFD approach is extended to accomplish long-term simulations (up to the microsecond scale) of large molecular ensembles (representing millions of atoms) containing phospholipid membranes, peptides, and proteins. For peptides and proteins a generally applicable fragmentation scheme is introduced in combination with specific backbone forces that keep native spatial shapes with adequate levels of flexibility or rigidity. The new approach is demonstrated by MFD simulations of the formation and characteristics of phospholipid membranes and vesicles, vesicle−membrane fusion, the backbone force dependency of the overall structural flexibility of dumbbell-shaped Calmodulin, the stability of subunit-aggregation of tetrameric hemoglobin, and the collaborative interaction of Kalata B1 cyclotides with a phospholipid membrane. All findings are in reasonable agreement with experimental as well as alternative simulation results. Thus, the extended MFD approach may become a new tool for biomolecular system studies to allow for comparatively fast simulative investigations in combination with a comparatively high chemical granularity.

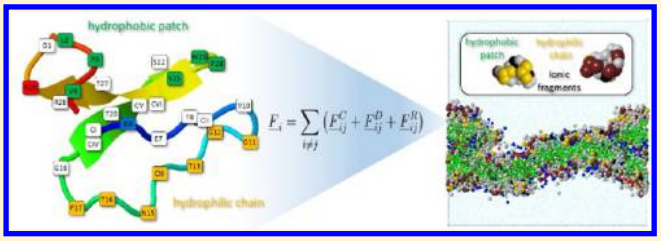

INTRODUCTION

Membranes, peptides, and proteins play an essential role in numerous biological structures and processes that can hardly be overestimated: Membranes achieve the division of cell compartments and take part in cellular transport and secretion, cell-to-cell recognition, or signal transduction. They serve as a container for membrane-bound proteins, form vesicles, and may fuse together.[1−3] As enzymes, proteins catalyze metabolic reactions; as receptors or transmitters, they play a predominant role in cell signaling and signal transduction; as transporters, they carry other molecular entities; and as structural proteins, they contribute to stiffness and rigidity.[4] In addition peptides and proteins are important ingredients in numerous (bio)-technical processes and (medical) products. The molecular composition of biological membranes consists of several sorts of phospholipid molecules where each phospholipid is a chemical amphiphile containing a hydrophilic "head" connected to a glycerol backbone with a fatty acid lipophilic "tail".[5−8] This amphiphilic character leads to their supramolecular alignment to form a bilayer structure with a hydrophobic core and a hydrophilic surface. The molecular 3D structures of peptides and proteins are mainly determined by the sequences of their amino acid building blocks which themselves are coded in the genes.[4]

Due to their sketched importance biological membranes, peptides, and proteins are eminent objects of study by both experimental and theoretical means as well as computer simulations in particular. A basic challenge for biomolecular simulations is the necessity to study comparatively large and complex structures in the order of at least tens of nanometers (leading to simulation boxes with hundred of thousands up to millions of atoms) for comparatively long times up to the microsecond scale. In addition a true understanding of molecular structure and (reactive) behavior would require an atomistic quantum−mechanical (QM) level of description. Although promising semiempirical approximations or combinations of quantum and molecular mechanics (QM/MM) are active fields of (protein) research,[9−12] a more general QM treatment with higher levels of theory is still completely out of scope due to the sketched system dimensions. Thus, atomistic membrane and peptide/protein modeling is mainly performed on the basis of approximate mechanical force fields to study

Received: October 9, 2014
Published: April 22, 2015

DOI: 10.1021/ci5006096
J. Chem. Inf. Model. 2015, 55, 983−997

structural properties and dynamical behavior with Molecular Mechanics (MM) and Molecular Dynamics (MD) respectively.[13−19] But even for an atomistic force-field level of approximation, there is often a need for high-performance computing facilities with still long simulation times in the order of weeks or even months. Atomistic approaches also require a detailed preparation with elaborate design software for adequate start geometries since hard atomic potentials are prone to entanglements and caging effects which can slow down the simulation progress or even lead to complete failure. These issues are a motivation for the development of mesoscopic coarse-grained techniques:[20−38] They try to remove the majority of "uninteresting" mechanical degrees of freedom from simulation (e.g., those related to pure solvent molecule movements) but to keep the essential dynamical behavior and structural characteristics of the complex system of interest. This reduction may decrease the computational costs by several orders of magnitude. Moreover it alleviates the geometric requirements for the design of adequate start geometries significantly since the coarse-grained interacting units may be represented by soft potentials which allow their mutual penetration so that problems like caging effects become less severe.[39] However, a mesoscopic approach will in general not be suitable for research fields that are based on precise atomistic interactions like protein−ligand docking or small-ligand virtual screening (although it may be applicable in special cases) but may be helpful to adequately describe average collaborative interactions in large molecular ensembles.

A well-established mesoscopic simulation technique is dissipative particle dynamics (DPD): This mesoscopic method was introduced in the early 1990s to describe the hydrodynamic behavior of complex fluids and soft matter systems by movement of adequate fluid elements (its particles or beads)[40,41] where DPD is basically neither an atomistic nor a molecular simulation technique since its particles may be arbitrarily defined fluid portions.[42] Molecular fragment dynamics (MFD) is a molecular DPD variant with beads that are chosen to be small molecules which may be connected by harmonic springs to represent larger molecular entities (and thus may be regarded as "fragments" of larger molecules), e.g., a small water molecule is represented by a single bead whereas a larger phospholipid molecule representation requires several connected beads. From a chemical point of view, MFD may be regarded as a chemically intuitive fine-grained variant of the intrinsically coarse-grained DPD simulation technique which maintains a comparatively accurate representation of the structure of molecules. MFD has already been successfully utilized for the study of amphiphilic polymers, microemulsions, and nonionic surfactant systems.[43−45]

It is the aim of this study to extend the MFD approach to biomolecular simulation of phospholipid membranes, peptides, and proteins to enrich the space of alternative simulation techniques for biomolecular research and development. As already pointed out above, MFD can not achieve the precision of atomistic (or coarse-grained) MD methods and thus will face a restricted field of application where only averaged interactions determine the system's behavior and structure of interest. On the other hand this principal limitation is being opposed by definite advantages to its more precise simulation teammates: The preparation of complete simulation setups with adequate molecular start configurations is comparatively easy and fast, and simulation times of scientifically relevant systems comprising millions of atoms toward equilibrium are very short—on the order of 10−100 h (overnight/overweekend) on a single core of contemporary notebook or workstation computers (thus hardware requirements are very humble and generally available)—and common pitfalls due to inappropriate start configurations, energy barriers, hindered motions, or local energy minima are considerably reduced because of the dynamical method's characteristics. These criteria are preferably valued in nonacademic and industrial environments where time and effort are crucial constraints. It should also be emphasized that the basic interaction parameters of all MFD fragments used in this work are derived in a general manner and are not manually adjusted to any specific simulation system of interest. To demonstrate the general applicability of the MFD technique for biomolecular simulation the following systems are considered: the formation and characteristics of pure 1,2-dimyristoyl-*sn*-glycero-3-phosphatidylcholine (DMPC) membranes as well as more biologically realistic models of endoplasmic reticulum (ER) and mitochondrial and plasma-like membranes are analyzed and compared to alternative simulation results as well as experiments. In addition vesicle formation and a DMPC vesicle−membrane fusion is investigated. For peptide/protein modeling in particular the following strategy is followed: (1) A set of adequate MFD fragments/beads is identified that comprises the "average chemistry" of all proteinogenic amino acids. (2) For each amino acid and possible dipeptide a fragmentation scheme is developed, i.e. an adequate decomposition of each molecular entity into its specific fragments/beads. (3) Since the conservative DPD/MFD bead interaction is a isotropic soft repulsion, a bead-based protein representation is in general not able to account for a stable spatial molecular 3D structure which is determined by anisotropic atomic interactions like hydrogen bonds that lead to secondary structures like α-helices or β-sheets. Thus, specific interactions between peptide/protein backbone beads are introduced to control structural flexibility or rigidity. Details of the sketched strategy are outlined and comprehensive MFD simulations are presented that demonstrate the influence of backbone forces to the overall structural flexibility of dumbbell-shaped calmodulin, the stability of subunit-aggregation of tetrameric hemoglobin, and the collaborative interactions of Kalata B1 cyclotides with a phospholipid membrane.

METHODS

Dissipative Particle Dynamics. DPD is a coarse-grained mesoscopic simulation technique for isothermal complex fluids and soft matter systems. It combines features from MD, Langevin dynamics, and Lattice-Gas Automata, satisfies Galilean invariance and isotropy, and conserves mass and momentum—thus DPD is expected to show correct hydrodynamic behavior and to obey the Navier−Stokes equations.[46−48] As its name indicates DPD is a particle-based method where a particle (bead) represents a fluid element or portion of the fluid of interest. The beads interact in an additive pairwise manner and move in discrete time steps through space where their movement is governed by Newton's equation of motion

$$\underline{F}_i = m_i \frac{\mathrm{d}\underline{v}_i}{\mathrm{d}t}, \qquad \underline{v}_i = \frac{\mathrm{d}\underline{r}_i}{\mathrm{d}t} \tag{1}$$

with time t, spatial position $\underline{r}_i$, velocity $\underline{v}_i$, mass m_i, and (total) force $\underline{F}_i$ acting on bead i. For integration, a modified Velocity−

DOI: 10.1021/ci5006096
J. Chem. Inf. Model. 2015, 55, 983−997

Verlet algorithm is used.[49,50] The force $\underline{F}_i$ consists of a conservative part $\underline{F}_{ij}^{C}$, a dissipative part $\underline{F}_{ij}^{D}$, and a random part $\underline{F}_{ij}^{R}$

$$\underline{F}_i = \sum_{i \neq j} (\underline{F}_{ij}^{C} + \underline{F}_{ij}^{D} + \underline{F}_{ij}^{R}) \tag{2}$$

where the sum is calculated over all pairs of beads within a limited distance. The conservative force $\underline{F}_{ij}^{C}$ is chosen to be a soft repulsion controlled by an isotropic repulsion parameter a_{ij} for a pair of beads i and j acting along their line of centers and is given by

$$\underline{F}_{ij}^{C} = \begin{cases} a_{ij}(1 - r_{ij})\hat{r}_{ij} & (r_{ij} < 1) \\ 0 & (r_{ij} \geq 1) \end{cases} \tag{3}$$

where $\underline{r}_{ij} = \underline{r}_i - \underline{r}_j$, $r_{ij} = |\underline{r}_{ij}|$, $\hat{r}_{ij} = \underline{r}_{ij}/|\underline{r}_{ij}|$. The dissipative part $\underline{F}_{ij}^{D}$ describes the friction that acts on the relative velocities of the beads:

$$\underline{F}_{ij}^{D} = -\gamma_{DPD}\omega^{D}(r_{ij})(\hat{r}_{ij}\cdot v_{ij})\hat{r}_{ij} \tag{4}$$

where v_{ij} is the relative velocity, γ_{DPD} is the friction coefficient, and $\omega^{D}(r_{ij})$ is the variation of the friction coefficient with distance. With only the dissipative/frictional force in place the beads would finally stop their relative motion after a slowing-down crossover. The random force $\underline{F}_{ij}^{R}$ opposes against the dissipative force by providing random "kicks" that keep the beads in motion:

$$\underline{F}_{ij}^{R} = \sigma\omega^{R}(r_{ij})\theta_{ij}\hat{r}_{ij} \tag{5}$$

where σ controls the magnitude of the random force, $\omega^{R}(r_{ij})$ describes its variation with distance, and θ_{ij} is a randomly fluctuating variable with Gaussian distribution and unit variance. The functions $\omega^{D}(r_{ij})$, $\omega^{R}(r_{ij})$, and the coefficients γ and σ cannot be chosen idependently from each other. Espanol and Warren[51] have shown that a DPD system is simulated in the canonical NVT-ensemble if the following two weight functions are defined:

$$\gamma_{DPD} = \frac{\sigma^2}{2k_B T} \tag{6}$$

$$\omega^{D}(r_{ij}) = [\omega^{R}(r_{ij})]^2 \tag{7}$$

where k_B is the Boltzmann constant and T the thermodynamic temperature. The interplay of random and dissipative part acts like a thermostat conserving the total momentum and introducing Brownian motion into the system. The DPD technique is designed to rigorously sample the canonical NVT-ensemble which allows for a comparatively high tolerance for different (and possibly nonoptimum) start geometries.[48,51−55]

Molecular Fragment Dynamics. For the setup of a DPD simulation the a priori definition of adequate beads and the determination of their a_{ij} repulsion parameters is mandatory. The molecular fragment dynamics (MFD) variant chooses the beads to be small molecules (as "fragments" of larger molecules) and determines the a_{ij} repulsion parameters with atomistic MD simulations comprising the small molecules/beads in question. This procedure is based on a linear relation of the a_{ij} repulsion parameters to the Flory−Huggins interaction parameters χ_{ij}[55]

$$a_{ij}(T) = 25 + 3.497\chi_{ij}(T) \tag{8}$$

which in turn are defined as

$$\chi_{ij} = \frac{Z_{ij}\Delta E_{ij}}{RT} \tag{9}$$

where Z_{ij} is the coordination number, R is the gas constant, T is the temperature, and ΔE_{ij} is the differential pair interaction energy

$$\Delta E_{ij} = \frac{1}{2}(E_{ij} + E_{ji}) - \frac{1}{2}(E_{ii} + E_{jj}) \tag{10}$$

The coordination numbers Z_{ij} as well as the pair-interaction energies E_{ij} can be obtained by atomistic MD simulations with the small molecules representing beads i and j respectively.[43−45,56,57] All MD simulations for a_{ij} parameter determination are carried out using the Condensed-phase Optimized Molecular Potentials for Atomistic Simulation Studies (COMPASS) force field.[58] COMPASS is one of the most accurate force fields for the calculation of molecular interactions in aqueous systems since it is specifically parametrized for the modeling of fluids where the contributions of nonbonding interactions are crucial.

In addition to the determination of the a_{ij} parameters a MFD simulation requires an adequate decomposition of all molecules into a corresponding set of connected fragments: Small molecules (like water or methanol) are represented by a single (water or methanol) fragment whereas larger molecules are represented by several suitable fragments connected by harmonic springs in an appropriate manner to represent their covalent bonding and molecular characteristics.

Electrostatic Interactions. Different methods have been developed to introduce electrostatic interactions into DPD theory:[39,59,60] They all replace point charges by spread charge distributions to maintain soft bead potentials and avoid artificially strong ion pairing. In this study a simple electrostatic ad-hoc procedure is followed to account for the presence of a comparatively small number of charged beads and their short as well as long-range interactions in simulation.

For short-range interactions the mutual a_{ij} repulsion parameters between two charged beads i and j are adjusted to be at the lower boundary (for differently charged beads) or at the upper boundary respectively (for equally charged beads) of all determined a_{ij} values of all uncharged pairs, i.e., an electrostatic interaction is assumed to be stronger than any other nonbonded bead interaction:

$$a_{(\text{charged}),(\text{charged})} = a_{\max} + \Delta$$

$$a_{(\text{charged}),(\text{charged})} = a_{\min} - \Delta$$

$$\text{with } \Delta = c_{\text{correct}}(a_{\max} - a_{\min}) > 0 \tag{11}$$

where c_{correct} is chosen to be 0.1. The a_{ij} repulsion parameters of charged/uncharged bead pairs are corrected with the assumption that a charged bead is less repulsive in comparison to water (the MFD reference bead) than the corresponding uncharged bead:

DOI: 10.1021/ci5006096
J. Chem. Inf. Model. 2015, 55, 983−997

$$a_{i(\text{charged}),H_2O} = a_{i(\text{uncharged}),H_2O} - \Delta_i$$

$$a_{\substack{j(\text{uncharged}),H_2O \\ i\neq j}} > a_{H_2O,H_2O}: a_{i(\text{charged}),j(\text{uncharged})} = a_{i(\text{uncharged}),j(\text{uncharged})} + \Delta_i$$

$$a_{\substack{j(\text{uncharged}),H_2O \\ i\neq j}} \leq a_{H_2O,H_2O}: a_{i(\text{charged}),j(\text{uncharged})} = a_{i(\text{uncharged}),j(\text{uncharged})} - \Delta_i$$

$$\text{with } \Delta_k = \alpha |a_{i(\text{uncharged}),H_2O} - a_{H_2O,H_2O}| > 0;\ 0 \leq \alpha \leq 1 \quad (12)$$

where α is chosen to be 1.0. To account for the long-range character of electrostatic interactions an effective electrostatic force $\underline{F}_{ij}^{E}$ of charged bead j at position $\underline{r}_j$ on charged bead i at position $\underline{r}_i$ (in DPD units)

$$\underline{F}_{ij}^{E} = \begin{cases} \dfrac{q_i^* q_j^*}{r_{ij}^2}\hat{r}_{ij} & |\underline{F}_{ij}^{E}| < F_{\text{limit}};\ r_{ij} < r_{\text{cutoff}} \\ F_{\text{limit}} & |\underline{F}_{ij}^{E}| \geq F_{\text{limit}};\ r_{ij} < r_{\text{cutoff}} \\ 0 & r_{ij} \geq r_{\text{cutoff}} \end{cases} \quad (13)$$

is added to the bead−bead interactions where q_i^* is the effective charge of bead i. The soft bead potential is maintained by definition of an arbitrary maximum limit value F_{limit} of the additional effective electrostatic force. For all simulations F_{limit} is chosen to be 100 (in DPD units) and the cutoff distance r_{cutoff} is chosen to be 5.0 (in DPD units) for computational efficiency.

The value of the effective charges q_i^* of 1.0 (in DPD units) is estimated by MFD simulations of methylammonium acetate salt pairs with charged beads (*f*SMILES notation:[61] ⟨MeNH2-P⟩⟨HAcN⟩) in water so that artificially strong ion pairing does not show up:[59] Simulations with a 1000 salt pairs in 10^5 water molecules with increasing effective charges are performed and the fragment-based radius of gyration of the salt pair is chosen as a measure for ion pairing. Figure 1 shows that for an effective

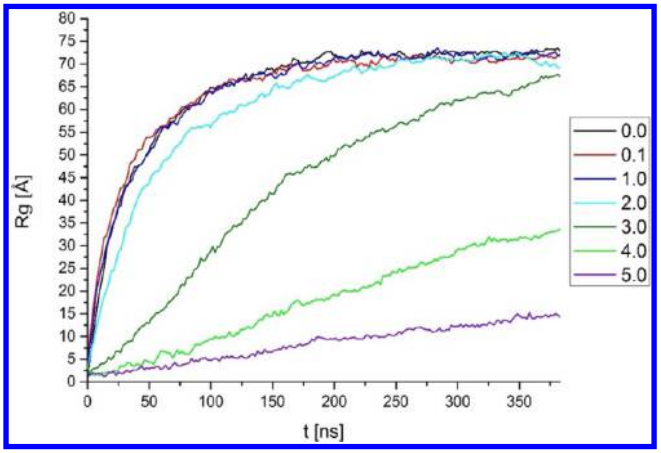

Figure 1. Fragment-based radius of gyration of the methylammonium acetate salt pairs during simulation for different effective charges of the salt beads.

charge up to 1.0 (DPD units) no distinct ion pairing in comparison to uncharged fragments occurs whereas for higher values ion pairing becomes more and more predominant with nonseparable ion pairs for an effective charge of 5.0.

MFD Fragment Set. For all simulations in this study a set of 34 beads/fragments with their mutual a_{ij} repulsion parameters is calculated at a (physiological) temperature of 310 K (see Table 1 with abbreviations, corresponding chemical names and effective charges and Figure 2 for a graphical representation of the a_{ij} repulsion parameters. The minimum a_{ij} value is set to 1.0 and the maximum a_{ij} value is 50.0. The diagonal element has a value of 27.0). It was an aim of the sketched MFD a_{ij} parameter determination procedure to generate a versatile set with a wide applicability to biomolecular modeling by consequent exclusion of any parameter adjustments due to specific application areas.

Table 1. List of Used Molecular Fragments

abbr	chemical name	charge
AcNH2	acetamide	0
HAc	acetic acid	0
Ph	benzene	0
Bu	butane	0
CisButene	cis-butene	0
DMP	dimethylphosphate	0
Et	ethane	0
EtOH	ethanol	0
EtNH2	ethylamine	0
Guanidine	guanidine	0
Imidazole	imidazole	0
Me	methane	0
MeSH	methanethiol	0
MeOH	methanol	0
MeAcNH	methyl acetamide	0
MeAc	methyl acetate	0
MeNH2	methylamine	0
PhOH	phenol	0
Pr	propane	0
PrOH	propanol	0
Pyrrole	pyrrole	0
Azolid	azolidine	0
H2O	water	0
ZnAc	zinc acetate	0
TriMeN	trimethylamine	0
HAcN	acetic acid	−1
DMPN	dimethylphosphate	−1
GuanidineP	guanidine	1
ImidazoleP	imidazole	1
MeSHN	methanethiol	−1
MeNH2P	methylamine	1
PhOHN	phenol	−1
AzolidP	azolidine	1
TriMeNP	trimethylamine	1

Membrane Compositions and Fragmentation. The phopholipid compositions of the four studied membrane types—denoted as (pure) DMPC, endoplasmic reticulum (ER), mitochondrial, and plasma-like[6]—are provided in Figure 3. The decomposition of the used phospholipid molecules into their molecular fragments/beads is given in Table 2 where the *f*SMILES notation is used which is described in a previous publication[61](see Figure 4 for a sketch of the fragmentation scheme of DMPC). The [START] and [END] tags are used for a linear start orientation of the corresponding molecules' geometries in the compartment editor of the simulation software. The coloring scheme of the molecules used for simulation box display is summarized in Table 3. The abbreviation PC comprises the four phospholipid variants DMPC, DPPC, DOPC, and POPC which are arbitrarily chosen

DOI: 10.1021/ci5006096
J. Chem. Inf. Model. 2015, 55, 983−997

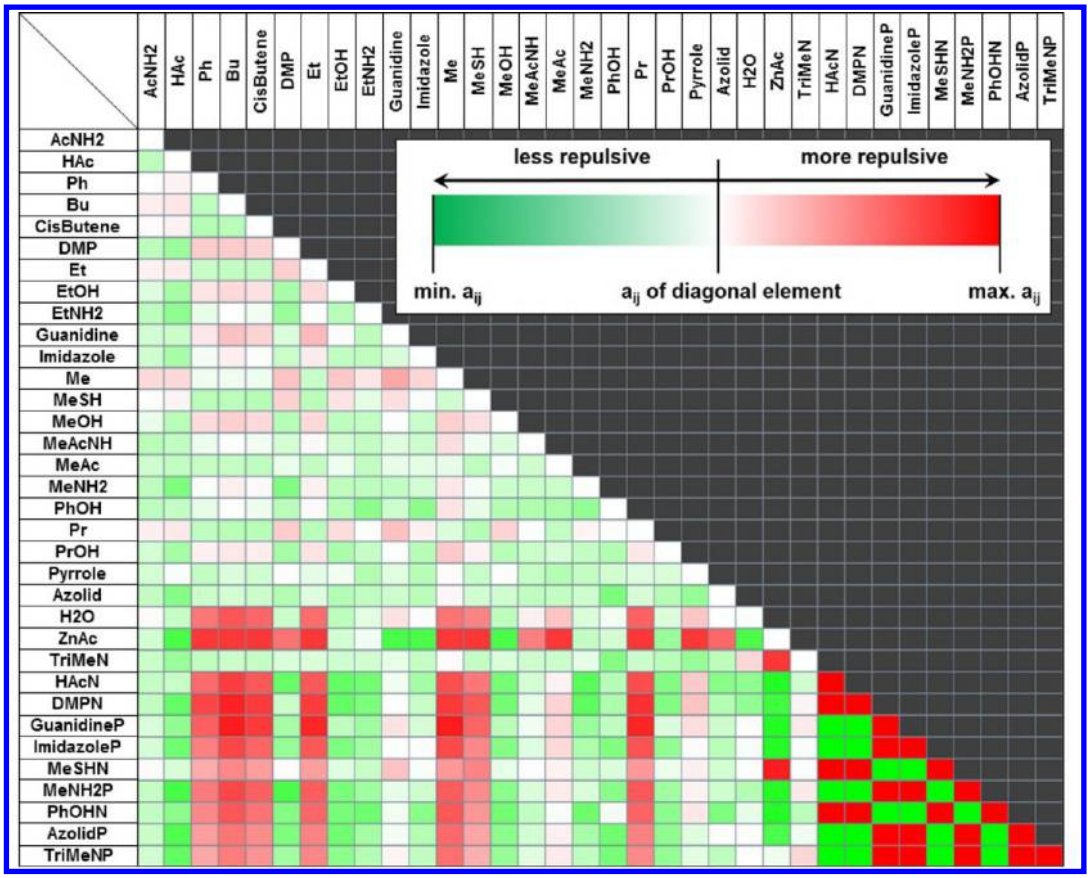

Figure 2. Graphical representation of the a_{ij} repulsion parameters.

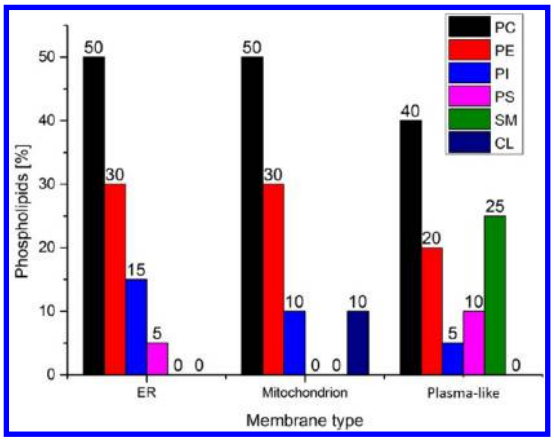

Figure 3. Lipid composition of the simulated membranes types.

in equal proportions. A biological plasma membrane contains up to 50% cholesterol: Since the used MFD fragment set does not contain the necessary fragments for an adequate fragmentation of this lipid, it is completely neglected and the corresponding membrane approximation is denoted as "plasma-like".

Peptide/Protein Fragmentation. The fragmentation schemes of all proteinogenic amino acids into their molecular fragments/beads are given in Table 4. Figure 5 illustrates the fragmentation scheme for the tripeptide arginine-isoleucine-serine (RIS) where the fragmentation from the N-terminus (methylamine fragment) along the peptide/protein backbone (methylacetamide fragments) to the C-terminus (acetic acid fragment) is shown.

The charge state of amino acids due to different pH values is represented by the use of correspondingly charged fragments, e.g. a neutral methylamine fragment at the N-terminus may be replaced by its cation with a positively charged amino group. Disulfide bridges are represented by connected methanethiol (MeSH) fragments. For peptides and proteins with loop sequences, the methylamine fragment at the N-terminus and the acetic acid fragment at the C-terminus are replaced by a connected methylacetamide (MeAcNHBB) fragment.

The sketched amino acid and peptide fragmentation schemes can be used to uniquely parse an arbitrary (protein) amino acid sequence at a defined pH value into a corresponding *f*SMILES representation to be used in an MFD simulation. In addition available protein 3D structure information may be used for the relative spatial positions of the protein backbone fragments in the simulation box. Both may be derived from Protein Data Bank (PDB) files.[62]

Protein Backbone Flexibility. Due to its isotropic conservative soft repulsion forces the DPD/MFD technique is in general not able to account for the anisotropic interactions that determine the stable spatial 3D geometry of proteins. Thus, geometric constraints have to be imposed on the relative positions of the molecular fragments/beads which a protein is represented with. The MFD approach in this study allows specific harmonic forces between protein backbone fragments to specify an arbitrary level of flexibility or rigidity whereas amino acid side-chain fragments do not encounter any restrictions. The maximum number N_{max} of possible harmonic forces between the backbone fragments is given by

DOI: 10.1021/ci5006096
J. Chem. Inf. Model. 2015, 55, 983−997

Table 2. Fragmentation Scheme of Phospholipid Molecules

membrane lipid	abbr	fragmentation scheme
1,2-dimyristoyl-*sn*-glycero-3-phosphatidylcholine	DMPC	TriMeNHP[START]-DMPN(MeAc-6Et)(MeAc-6Et[END])
1,2-dipalmitoyl-*sn*-glycero-3-phosphatidylcholine	DPPC	TriMeNHP[START]-DMPN(MeAc-8Et)(MeAc-8Et[END])
1,2-dioleoyl-*sn*-glycero-3-phosphatidylcholine	DOPC	TriMeNHP[START]-DMPN(MeAc-Et-Pr-CisButene-3Et-Pr)(MeAc-Et-Pr-CisButene-3Et-Pr[END])
2-oleoyl-1-palmitoyl-*sn*-glycero-phosphatidylcholine	POPC	TriMeNHP[START]-DMPN(MeAc-8Et)(MeAc-Et-Pr-CisButene-2Et-Pr[END])
2-oleoyl-1-palmitoyl-*sn*-glycero-phosphatidylethanolamine	PE	MeNH2P[START]-DMPN(MeAc-Et-Pr-CisButene-2Et-Pr)(MeAc-8Et[END])
1,3-bis(1′,2′-dilinoleoyl-*sn*-glycero-3′-phospho)-*sn*-glycerol	CL	DMPN(MeAc-Et-Pr-CisButene-CisButene-2Et)(MeAc-Et-Pr-CisButene-CisButene-2Et)-MeOH[START]-DMPN(MeAc-Et-Pr-CisButene-CisButene-2Et)(MeAc-Et-Pr-CisButene-CisButene-2Et[END])
[(2*R*)-1-[hydroxy-[(1*R*,2*R*,3*S*,4*R*,5*R*,6*S*)-2,3,6-trihydroxy-4,5-diphosphonooxycyclohexyl] oxyphosphoryl]oxy-3-octadecanoyloxypropan-2-yl](5*Z*,8*Z*,11*Z*,14*Z*)-icosa-5,8,11,14-tetraenoate	PI	DMPN[1](MeAc-8Et)(4 CisButene-Et[START])-MeOH-DMPN-DMPN[END]-MeOH−MeOH[1]
1,2-octadecanoyl-*sn*-glycero-3-phosphoserine	PS	HAcN[START](MeNH2P)-DMPN(MeAc-9Et)(MeAc-9Et[END])
Sphingomyelin	SM	TriMeNHP[START]-DMPN(MeAcNH2-7Et)(MeOH-CisButene-6Et[END])

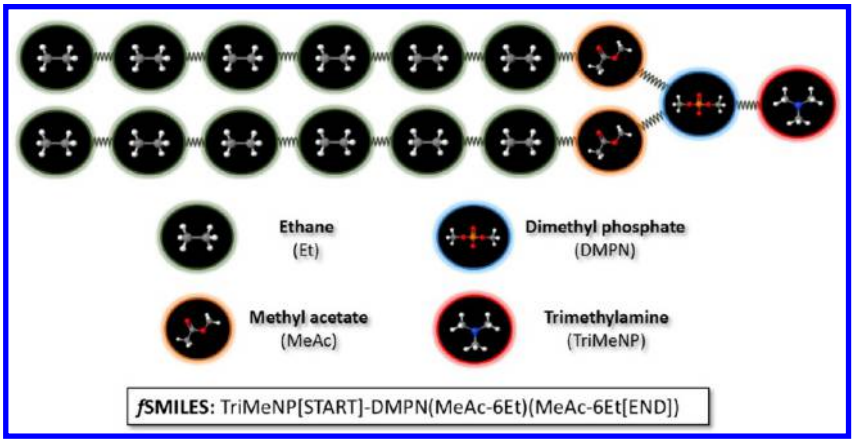

Figure 4. Fragmentation scheme and corresponding *f*SMILES of the charged membrane lipid DMPC.

Table 3. Colouring Scheme of Membrane Lipid Head Group Fragments[a]

membrane type	color of headgroup
DMPC	blue (DMPN), red (TriMeNHP)
DPPC	blue (DMPN), red (TriMeNHP)
DOPC	blue (DMPN), red (TriMeNHP)
POPC	blue (DMPN), red (TriMeNHP)
POPE	gold (DMPN), orange (MeNH2P)
CL	cobalt (DMPN), indigo (MeOH)
PIP2	violet (DMPN), magenta (MeOH)
PS	olive (HAcN, DMPN), mint (MeNH2P)
SM	brown (DMPN), gray (TriMeNHP)

[a]All other fragments are green.

$$N_{max} = \frac{(N_{AA} - 1)N_{AA}}{2} \quad (14)$$

where N_{AA} is the number of amino acids in the protein. Figure 6 illustrates single "1−3" to "1−6" backbone forces for the decorbin-binding protein A (PDB ID: 2LQU[63]) which consists of 168 amino acids, thus N_{max} is 14028. The "1−x" notation means that there are $(x - 1)$ backbone fragments between the interacting pair of fragments, i.e. for a protein with N_{AA} amino acids a number of $(N_{AA} - 1)$ "1−2" harmonic forces may be imposed, but there is only one single possible "1−N_{AA}" interaction.

The strength of a harmonic force between two backbone fragments may be defined by an individual force constant k_{BB} to allow for continuous levels of flexibility (small value range) or rigidity (large value range).

Simulations. All simulations of this study are performed with the simulation software MFD-FormulaOne:[64] This rich-client application comprises a fast MFD simulation kernel developed by CAM-D Technologies[65] (already applied stand-alone to several industrial projects[44,45,57,66] and as part of MFD-FormulaOne to study nonionic surfactants at the water−air interface in a recent work[43]) which is framed by a molecular fragment cheminformatics software layer developed according to Truszkowski et al.[61] (that among other features implements the *f*SMILES notation to describe single molecule fragmentations) and wrapped by a graphical user interface. MFD-FormulaOne may operate with different fragment sets where the specific fragment set related information has to be provided in form of a structured ASCII file. The application allows the design, execution, and analysis of MFD simulation jobs in an integrated all-in-one manner where peptide and protein editors allow specific settings (e.g., charge settings due to a specific pH value, backbone potential ranges/exclusions, amino acid exchange) as well as an import and automated conversion of PDB files into adequate *f*SMILES with corresponding protein 3D structure information. All simulation settings used in this study are described in Tables 5, 6, and 7 where additional

DOI: 10.1021/ci5006096
J. Chem. Inf. Model. 2015, 55, 983−997

Table 4. Fragmentation Scheme of All Proteinogenic Amino Acids[a] Suffix BB denotes backbone fragments

1-letter	3-letter	amino acid	*f*SMILES
A	Ala	alanine	MeAcNHBB(Me)
R	Arg	arginine	MeAcNHBB(Pr-Guanidine)
N	Asn	asparagine	MeAcNHBB(AcNH2)
D	Asp	aspartic acid	MeAcNHBB(HAc)
C	Cys	cysteine	MeAcNHBB(MeSH)
E	Glu	glutamic acid	MeAcNHBB(Me-HAc)
Q	Gln	glutamine	MeAcNHBB(Me-AcNH2)
G	Gly	glycine	MeAcNHBB
H	His	histidine	MeAcNHBB(Me-Imidazole)
I	Ile	isoleucine	MeAcNHBB(Et-Et)
L	Leu	leucine	MeAcNHBB(Me-Pr
K	Lys	lysine	MeAcNHBB(Pr-MeNH2)
M	Met	methionine	MeAcNH(Et-MeSH)
F	Phe	phenylalanine	MeAcNHBB(Me-Ph)
P	Pro	proline	AzolidBB
S	Ser	serine	MeAcNHBB(MeOH)
T	Thr	threonine	MeAcNHBB(PrOH)
W	Trp	tryptophan	MeAcNHBB(Me-Pyrrole-Ph)
Y	Tyr	tyrosine	MeAcNHBB(Me-PhOH)
V	Val	valine	MeAcNHBB(Pr)

[a] *f*SMILES corresponds to amino acids in peptides/proteins. The C- and N-terminal backbone fragments are exchanged with HAcBB and MeNH2BB respectively.

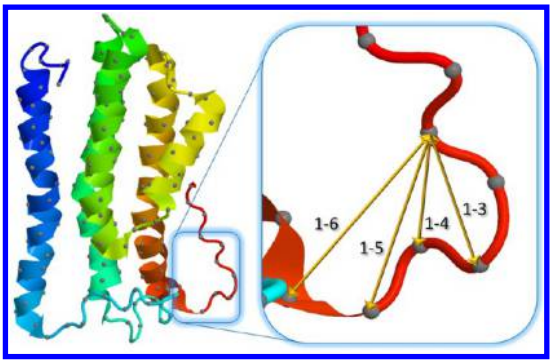

Figure 6. Possible harmonic 1−3 to 1−6 forces between backbone fragments (in gray).

Table 5. General MFD Engine Parameters

parameter	value [DPD units]
Standard Settings	
time step period	0.04
dissipative force steps	5
temperature steps	100
temperature	310 [K]
Electrostatic Interactions	
cutoff (r_{cutoff})	5.0
maximum absolut value (F_{limit})	100
effective charge (q^*)	1.0

information is provided in the text. All findings are obtained with the graphical and measurement functions provided by the simulation system. The simulation times on a single processor core of a contemporary Intel i7 or Xeon E5 processor range from the order of 10 h for the smaller membrane and protein systems to the order of 100 h for the larger vesicle−membrane and Kalata-B1−membrane systems. The memory consumption is less than 100 MB for the smaller and less than 1 GB for the larger simulations. For an average trained user the necessary preparation time for a complete "click-by-click" simulation job setup of is always in the order of minutes for all simulations performed.

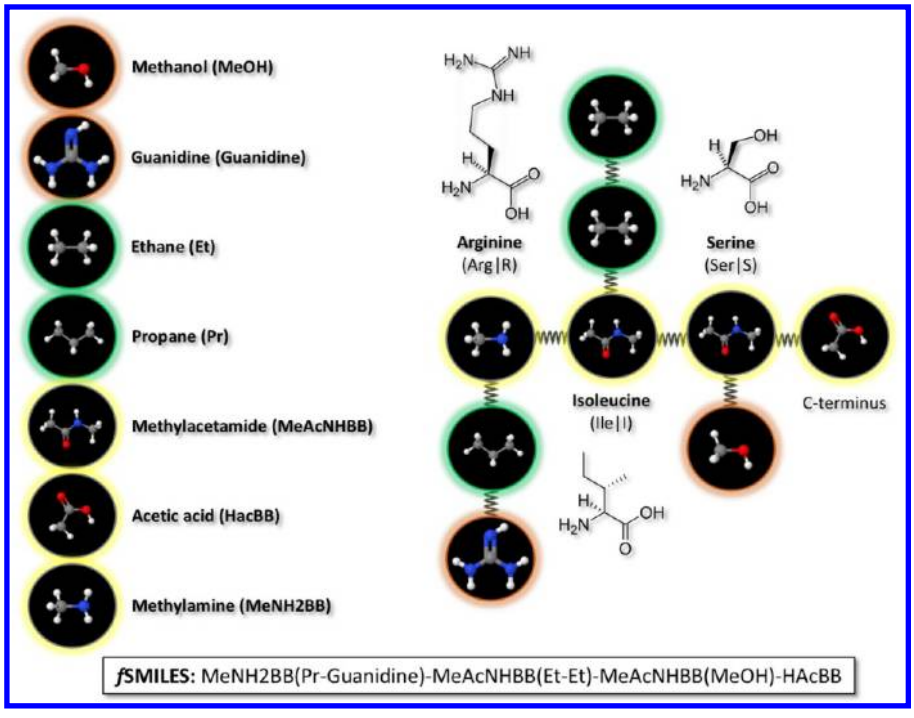

Figure 5. (left) Molecular fragments/beads: (red) hydrophilic, (green) hydrophobic, (yellow) backbone. The BB suffix denotes peptide/protein backbone fragments. (right) Fragmentation scheme of the tripeptide RIS from N-terminus to C-terminus. (bottom) Corresponding *f*SMILES notation.

DOI: 10.1021/ci5006096
J. Chem. Inf. Model. 2015, 55, 983−997

Table 6. Simulation Parameters for Membranes

parameter	Value [DPD units]
Stable Bilayer Membranes	
PBC $x/y/z$	on/on/on
box size	$32 \times 32 \times 32$ [nm^3]
number of phospholipids	1600
number of water molecules	2×10^5
simulation time steps	2×10^4
Intrabilayer Lipid Flips	
PBC $x/y/z$	on/on/on
box size	$32 \times 32 \times 32$ [nm^3]
number of phospholipids	1600
number of water molecules	2×10^5
simulation time steps	5×10^4
initial minimization steps	300
Vesicle Formation	
PBC $x/y/z$	on/on/on
box size	$30 \times 30 \times 30$ [nm^3]
number of phospholipids	1200−400
number of water molecules	2×10^5
simulation time steps	2×10^4
Vesicle Formation by Self-Assembly	
PBC $x/y/z$	on/on/on
box size	$35 \times 35 \times 35$ [nm^3]
number of phospholipids	1800
number of water molecules	2×10^5
simulation time steps	2×10^5
DMPC Vesicle−Membrane Fusion	
PBC $x/y/z$	on/on/off
box size	$51 \times 51 \times 51$ [nm^3]
number of phospholipids (membrane)	4000
number of phospholipids (vesicle)	4000
number of water molecules (vesicle)	4×10^4
number of water molecules	8×10^5
simulation time steps	4×10^4

Table 7. Simulation Parameters for Proteins

parameter	value [DPD units]
Backbone Forces and Flexibility of Calmodulin	
PBC $x/y/z$	on/on/on
box size	$18 \times 18 \times 18$ [nm^3]
number of water molecules	5×10^4
number of calmodulin molecules	1
simulation time steps	2×10^4
backbone stabilization constant (k_{BB})	0−10
Stability of Subunit Aggregation of Hemoglobin	
PBC $x/y/z$	on/on/on
box size	$23 \times 23 \times 23$ [nm^3]
number of water molecules	1×10^5
number of hemoglobin molecules	1
simulation time steps	1×10^6
backbone stabilization constant (k_{BB})	2
Interaction of Kalata B1 Cyclotides with a Plasma-like Membrane	
PBC $x/y/z$	on/on/on
box size	$32 \times 32 \times 32$ [nm^3]
number of Kalata B1 molecules	216 (unless otherwise noted)
number of phospholipids	1600
number of water molecules	2×10^5
Simulation time steps	4×10^5
backbone stabilization constant (k_{BB})	0.1

RESULTS AND DISCUSSION

Bilayer Membranes. For the membrane models cubic simulation boxes of size 32 nm × 32 nm × 32 nm are constructed which contain 2×10^5 water molecules. The lipids are randomly aligned in bilayer form in a xy-layer compartment due to their [START]/[END] tags as a start geometry (see Figure 7a). Periodic boundaries are turned on in all directions. All simulations are run for 1.7 μs to demonstrate the stability of

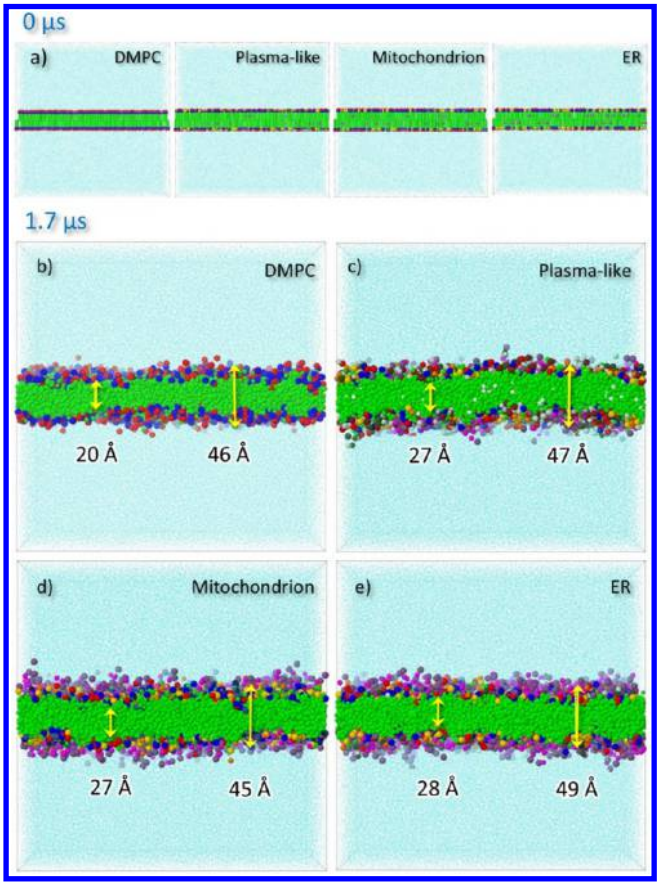

Figure 7. (a) Start geometries for DMPC, plasma-like, mitochondrial, and ER membrane bilayers. (b−e) Cross sections of all membranes after 1.7 μs of simulation.

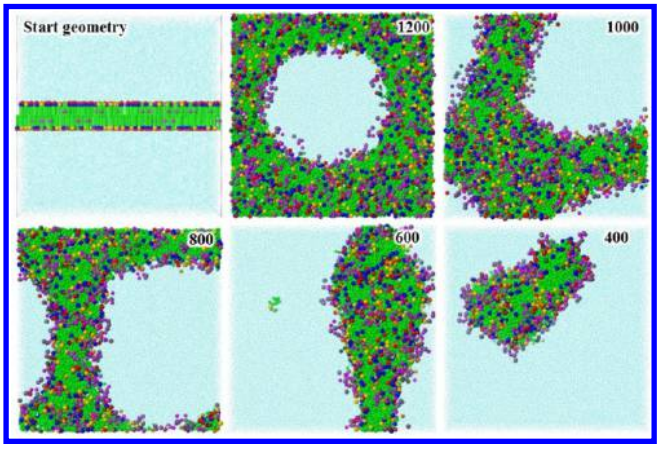

Figure 8. Start geometry (side view) and results (top view) for the ER membrane type (1200−400 lipid molecules) after a simulation time of 1.5 μs.

DOI: 10.1021/ci5006096
J. Chem. Inf. Model. 2015, 55, 983−997

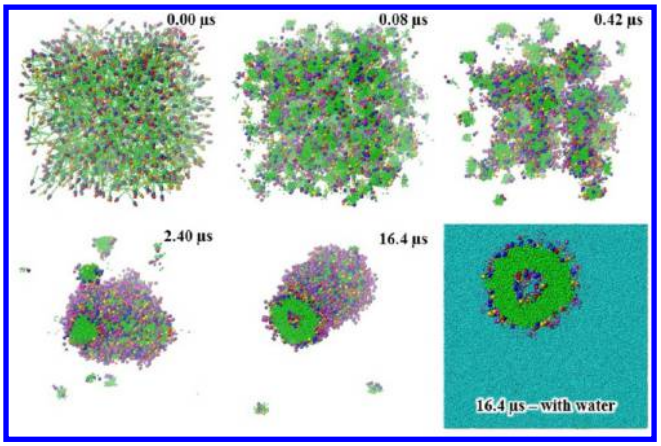

Figure 9. Simulation of 1800 mitochondrial lipids with random start geometry for 16.4 μs (water is not shown). (bottom right with water): Visualization of enclosed vesicle water.

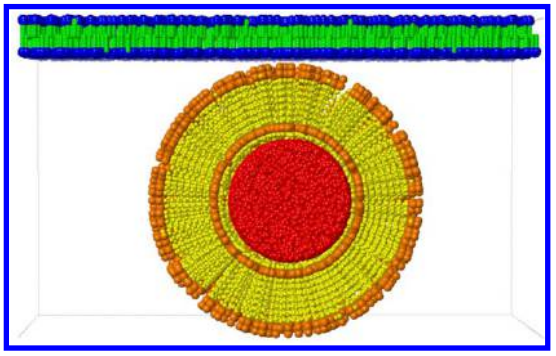

Figure 10. Start geometry of the DMPC membrane: (blue) head group fragments, (green) hydrophobic fragments. Vesicle bilayers: (orange) head group fragments, (yellow) hydrophobic fragments. The water molecules inside the vesicle are colored in red; bulk water is not shown.

the membrane model without any defects or wholes. The known experimental area per lipid of 60.7 ± 0.5 Å^2 of a DMPC membrane[67] can be approximately modeled with 1600 DMPC molecules for the chosen system size (which leads to an area per lipid of 60.5 Å^2). The other membrane types are also assembled with 1600 lipid molecules. The membrane thicknesses are measured with the simulation box measurement tools of the used simulation system (which allows arbitrary box orientations, fragment exclusions as well as parallel-projected through-space measurements) and thus contains the visual fuzziness of a few angstroms or approximately 10% of the reported values. For hydrophobic thickness measurements only the hydrophobic membrane fragments are taken into account (which corresponds to the thickness of the water fragment exclusion layer), for the overall thickness all membrane related fragments are considered. The DMPC, plasma-like, mitochondrial and ER membrane approximations show hydrophobic thicknesses of 20, 27, 27, and 28 Å and overall thicknesses of 46, 47, 45, and 49 Å (Figure 7b–e). These values are in agreement with experimental results (hydrophobic thicknesses of 19 ± 1 Å for DMPC membranes with a chain length of 12 carbon atoms[68] and about 30 Å for the other membranes types[6,69,70] as well as overall thicknesses of 40–50 Å[71,72]). All membranes studied exhibit the known wavelike surface fluctuations as well as occasional membrane curvatures.[73]

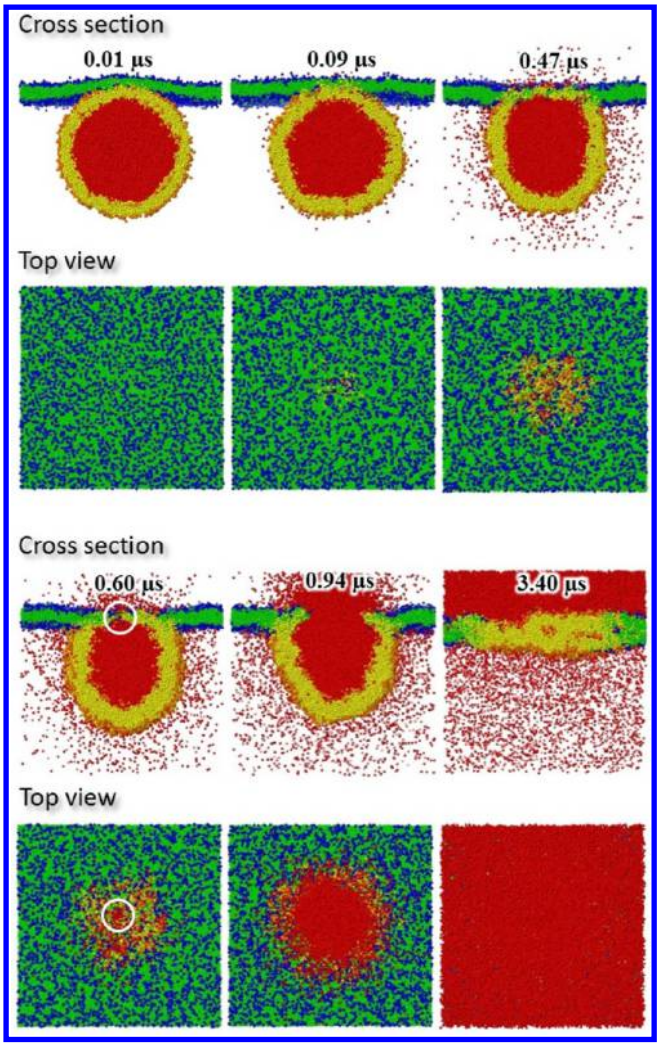

Figure 11. Fusion pathway of a DMPC vesicle with a DMPC membrane in cross section and top view.

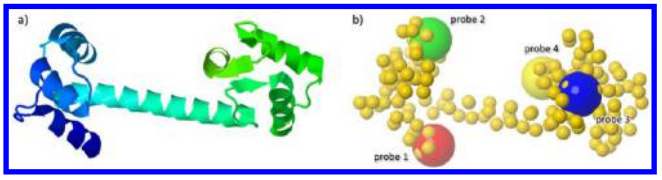

Figure 12. (a) Cartoon model of the dumbbell shaped protein calmodulin. (b) Positions of the probe fragments (red, green, blue, yellow) for geometry related calculations within the protein backbone (orange).

Intrabilayer Lipid Flips. Biological membranes are known for intrabilayer lipid exchange (so-called lipid flip-flops),[74−77] i.e. the ability of a phospholipid molecule to turn over from one layer of the bilayer structure to the other. For the stable membrane models described in the previous section these lipid flip-flops are investigated in a qualitative manner since a soft-potential DPD technique like MFD is not expected to yield a correct quantitative timely behavior of these processes. All membranes studied exhibit the expected phospholipid flip-flop transitions where the detected mobility rate is decreasing in the order DMPC, mitochondrial, ER, and plasma-like membrane (with relative rates of 2.2:1.6:1.4:1) to attempt at least a comparative quantitative assessment.

DOI: 10.1021/ci5006096
J. Chem. Inf. Model. 2015, 55, 983−997

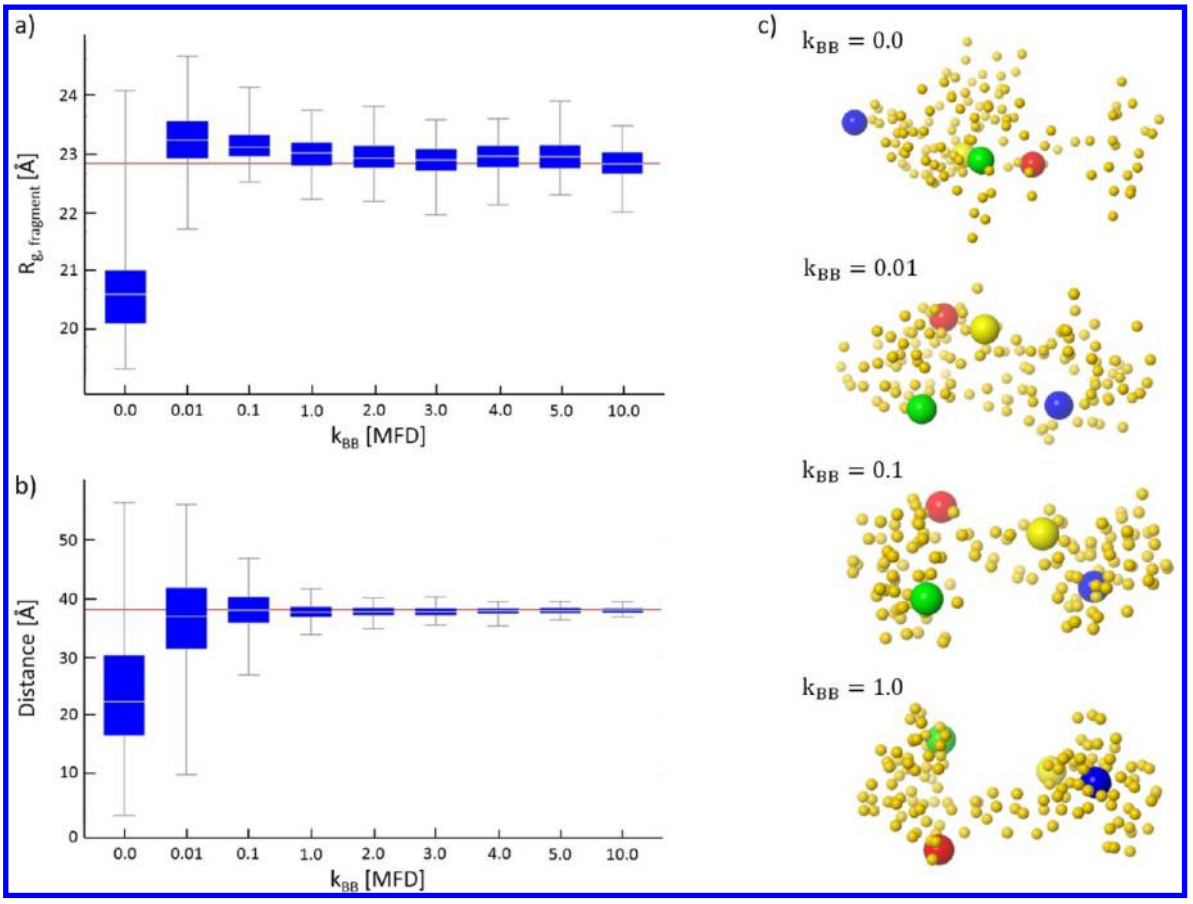

Figure 13. (a) Box-whisker-plot of $R_{g,fragment}$ against the force constants k_{BB}. (b) Box-whisker-plot of the distance between backbone probe fragments 1 and 3. The red line denotes the mean value of the simulation with the most conserved protein structure (highest k_{BB} value). (c) Structure of calmodulin after a simulation time of 1.5 μs for different force constants k_{BB}.

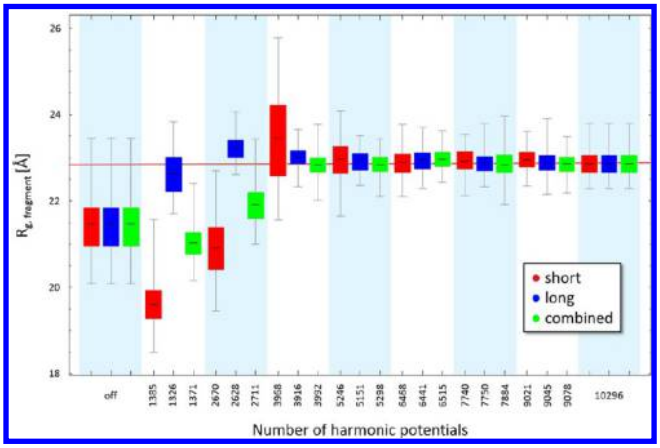

Figure 14. Box-whisker-plot of $R_{g,fragment}$ in dependence on the number of active backbone potentials for short, long, and combined potentials. The red line denotes the mean value of the full set of possible backbone potentials.

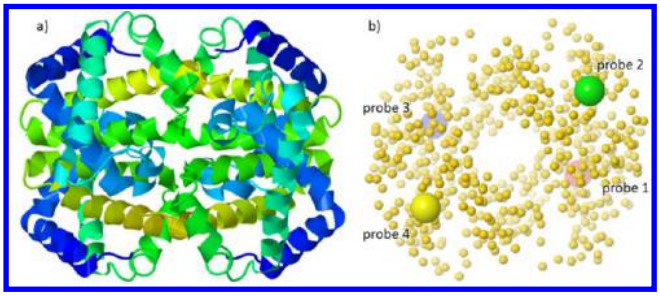

Figure 15. (a) Cartoon model of the quartery structure of hemoglobin. (b) Positions of the probe fragments (red, green, blue, yellow) within the protein backbone fragments (orange).

Vesicle Formation. The ability to form vesicles is a common characteristics of phospholipids with a critical packing parameter between 0.5 and 1.0.[78−81] In order to study vesicle formation with the phospholipid compositions of the different membrane types the total phospholipid amount of the simulations with bilayer start geometries in *xy*-layer compartments described above was successively decreased from 1200 to 400 molecules by constant relative composition of the different phospholipids: All membrane types show a crossover from a stable bilayer structure over a (branched) tube system to a final vesicle formation (see Figure 8 for a ER membrane). Alternatively spontaneous vesicle formation is analyzed with a random initial distribution of the phospholipids in the simulation box. Again vesicles are formed by self-assembly for all studied membrane compositions (see Figure 9 for the mitochondrial membrane composition simulated with 3×10^5 water and 1800 phospholipid molecules for 16.4 μs).

Vesicle−Membrane Fusion. The fusion of a vesicle with a membrane is studied for the DMPC lipid: The start geometry is a simulation box with 8×10^5 bulk water molecules that consists of a stable DMPC bilayer membrane with 4000 lipid molecules and an underlying DMPC bilayer vesicle of 4000

DOI: 10.1021/ci5006096
J. Chem. Inf. Model. 2015, 55, 983−997

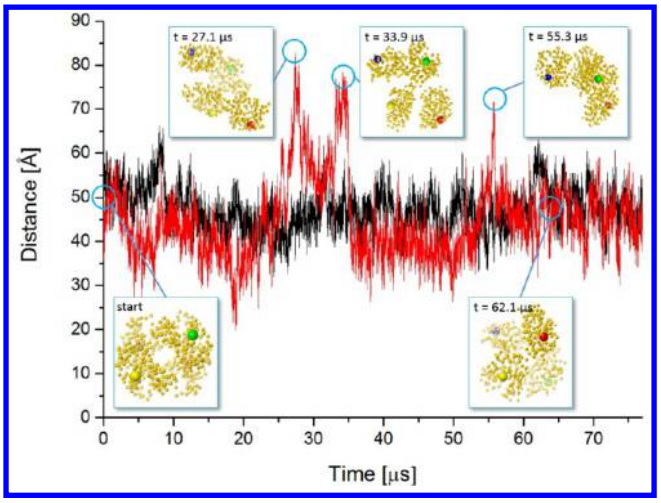

Figure 16. Distances between probes 1−2 (black) and probes 1−3 (red) during simulation. Some views of corresponding hemoglobin structures are depicted in the inset images.

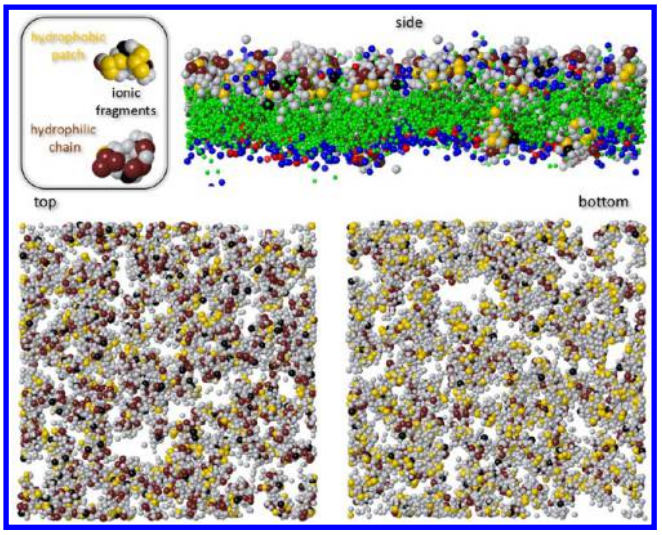

Figure 18. (upper left) Coloring scheme of Kalata B1. (upper right and bottom) Side, top, and bottom view of 144 Kalata B1 molecules in interaction with a plasma-like membrane. The membrane of the bottom images is hidden for better view of the Kalata B1 orientation.

lipid molecules (2200 outer, 1800 inner) filled with 4.5×10^4 water molecules constructed by an adequate overlay of xy-layer and sphere compartments. The start geometry is shown in Figure 10. The size of the simulation box is 51 nm × 51 nm × 51 nm, and the diameter of the vesicle is 30 nm. After 0.01 μs the diffusion of the vesicle leads to a first contact with the membrane which is pushed upward due to the mechanical impact (see Figure 11). With a growing contact area the first interbilayer lipid flips between vesicle and membrane are observed at 0.09 μs. The known leakage of water molecules from inside the vesicle through the vesicle's bilayer also becomes visible.[33] After 0.47 μs the enlarged contact area now exhibits a diffusive leakage of inner-vesicle water molecules through the membrane. At 0.60 μs a fusion pore is formed which grows in size to about 10 nm so that increasing amounts of inner-vesicle water pour out into the bulk volume above the membrane. Finally, after 3.40 μs the DMPC membrane and vesicle bilayers are fused. The duration of the described fusion process of about a few microseconds should not be regarded as a reliable quantitative estimate although it takes place in the correct order of magnitude compared to experimental results[82,83] and corresponds to findings of alternative DPD simulation approaches.[33]

Backbone Forces and Flexibility of Calmodulin. In order to study the influence of the harmonic forces between backbone fragments on the 3D protein structure the calcium-binding messenger calmodulin (PDB ID: 4BW8[84]) is chosen (see Figure 12): Its N- and C-terminal domains are separated by an α-helix which consists of 27 amino acids so that Calmodulin has an overall dumbbell shape. At simulation start a single Calmodulin protein with its backbone fragments at relative positions that correspond to its crystal structure and a charge state that corresponds to the physiological pH 7.4 is centrally placed into a box cosisting of 5×10^4 water fragments. In addition there are four backbone probe fragments positioned in each of the two terminal domains which are used for geometry related calculations (see Figure 13). The simulation is run for 1.5 μs. As a measure of the overall spatial protein geometry the fragment-based radius of gyration $R_{g,fragment}$ is calculated (note that $R_{g,fragment}$ inevitably slightly differs from the atomic radius of gyration R_g of 21.5 Å[85]). Figure 13a shows the influence of the force constant k_{BB} on the overall 3D geometry as measured by $R_{g,fragment}$ if all 10 296 possible harmonic forces between backbone fragments are activated with all the same strength, i.e. the same k_{BB} value (the deviations shown in the box-whisker-plot are a measure for the geometric flexibility of the protein structure when equilibrium is reached after 0.4 μs): A complete neglect of backbone forces

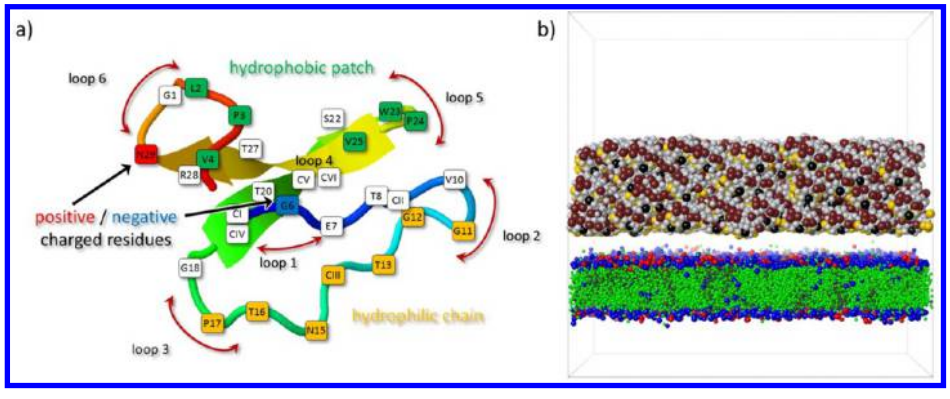

Figure 17. (a) Superposition of the cartoon model and the molecular structure of Kalata B1. (b) Start geometry for MFD simulations with a Kalata B1 layer above a membrane layer.

DOI: 10.1021/ci5006096
J. Chem. Inf. Model. 2015, 55, 983−997

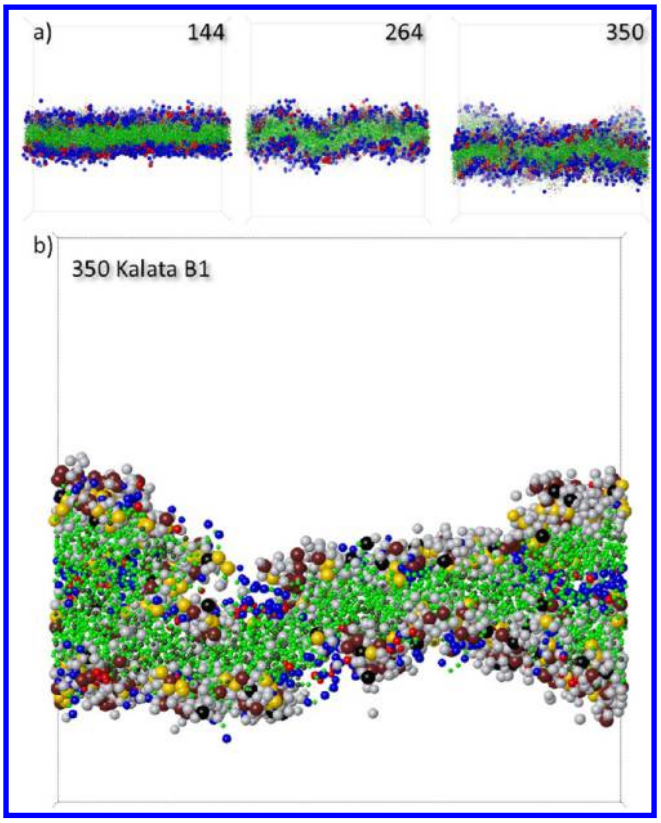

Figure 19. (a) Simulations box cross sections with increased membrane curvature due to an increased number of Kalata B1 cyclotides. (b) Depiction of the lipid extraction capability of 350 Kalata B1 cyclotids.

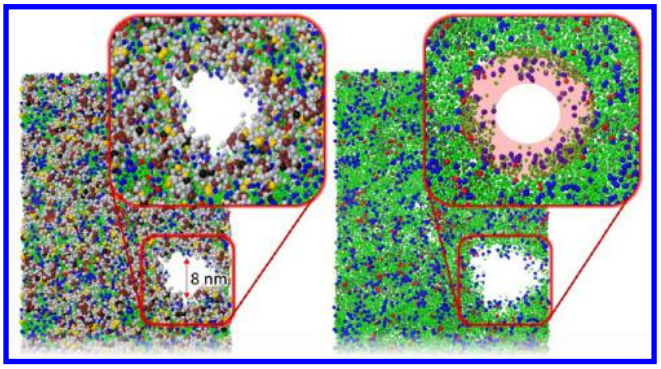

Figure 20. Membrane pore. (left) All water molecules are omitted. (right) Kalata B1 and water molecules are omitted to allow a view on the membrane lipid orientation. The red ring indicates the missing Kalata B1 cyclotids.

(k_{BB} = 0.0) leads to an expected collapse of the α-helix with globular protein conformations indicated by $R_{g,fragment}$ values which are significantly smaller than the one for the known dumbbell structure. For a very small value of k_{BB} = 0.01 the crystal geometry is already kept on average although there are strong fluctuations. Higher k_{BB} values preserve the crystal geometry with a decreasing level of flexibility for increasing force strengths. The distances between backbone probe fragments 1 and 3 confirm these findings (see Figure 13b). Figure 13c shows simulation box cross sections with the magnified Calmodulin structure for different k_{BB} values.

In general it is not necessary to activate all possible backbone fragment potentials to keep a 3D protein structure stable on average during simulation thus in practice the number of activated backbone potentials may be considerably reduced compared to the possible full set where the specifics have to be evaluated in each single case. Figure 14 shows that for calmodulin long-range backbone potentials play a more dominant role for the preservation of the 3D protein structure than the shorter ones—which may be taken as a generalized rule of thumb.

Stability of Subunit Aggregation of Hemoglobin. Hemoglobin (PDB ID: 2HHB[86]) consists of a quaternary structure with four subunits that do not contain any interunit covalent bonding (Figure 15a). To analyze the MFD long-term stability of the quaternary structure a single hemoglobin molecule with its backbone fragments at relative positions that correspond to its crystal structure and a charge state that corresponds to pH 7.4 is centrally placed in a box with 10^5 water fragments where only the tertiary structures of the subunits are stabilized by (all possible) backbone harmonic forces with a force constant of k_{BB} = 2.0, i.e. there are no constraints applied to the relative positions of the whole subunits. In addition each subunit contains a probe backbone fragment for geometry related calculations (highlighted by size in Figure 15b). The fragment-based radius of gyration $R_{g,fragment}$ as a function of simulation time oscillates around 28.5 Å (comparable to the experimental atomistic radius of gyration of R_g = 29 ± 2 Å[87]), i.e. the quaternary Hemoglobin structure is globally stable during a simulation of 76.5 μs. This is confirmed by a detailed analysis of distances and angles of the probe backbone fragments although intermediate conformations show distinct deviations from the crystal structure (see Figure 16).

Membrane Interaction of Kalata B1 Cyclotides. Kalata B1 is a cyclic disulfide rich peptide with 29 amino acids that belongs to the family of cyclotids which are known for their cytotoxic activity due to their destructive interaction with biological membranes.[88−91] The molecular structure of Kalata B1 (PDB ID: 1NB1[92]) is sketched in Figure 17a. The high affinity to lipid membranes can be traced to the hydrophobic patch formed by loop 6 (L_2, P_3, and V_4) as well as loop 5 (W_{23}, P_{24}, and V_{25}) and the ionic amino acids G_6 in loop 1 plus N_{29} in loop 6 that interact with the hydrophilic head groups of phospholipid molecules of the membrane. The interaction of Kalata B1 with a plasma-like phospholipid membrane is studied with a start geometry depicted in Figure 17b: A layer of 216 randomly positioned Kalata B1 molecules is located above a plasma-like membrane layer in a box of 2 × 10^5 water fragments. Each Kalata B1 as well as each phospholipid molecule is charged according to pH 7.4 and its 3D structure is stabilized by all possible backbone harmonic forces with a small force constant of k_{BB} = 0.1 to allow for conformational flexibility. The Kalata B1 coloring scheme is given in Figure 18 where the hydrophobic patch is yellow, the ionic residues are black and the hydrophilic chain is brown. Figure 18 shows the side, top and bottom view of the interactive membrane orientation of Kalata B1: The fragments of the hydrophobic patch prefer the hydrophobic membrane domain whereas the hydrophilic chain and the charged fragments are located at the hydrophilic membrane−water interface which corresponds to experimental and alternative simulation results.[88,93−97] An increasing number of Kalata B1 proteins leads to an increased curvature of the plasma-like membrane as demonstrated in Figure 19a with a lipid extraction from the membrane for higher Kalata B1 concentrations (see Figure 19b with an extracted lipid column up to a lipid inclusion by Kalata B1

DOI: 10.1021/ci5006096
J. Chem. Inf. Model. 2015, 55, 983−997

cyclotids). Lipid extraction may finally cause a membrane disruption by a formation of pores (see Figure 20) where a pore is stabilized by aligned Kalata B1 cyclotids with their hydrophobic patches oriented toward the membrane and their hydrophilic parts directed to the inner core of the pore. This behavior indicates a toroidal pore structure.[98] All findings are in agreement with experimental as well as alternative simulation results.[95,99]

CONCLUSION

As a molecular DPD variant molecular fragment dynamics may be successfully utilized to accomplish fast long-term simulations of large molecular ensembles containing phospholipid membranes and peptides/proteins with a comparatively high chemical granularity that are in reasonable agreement with experimental findings as well as alternative simulation results. For peptides and proteins a generally applicable fragmentation scheme is provided whereas their specific spatial conformations have to be stabilized by adequate backbone forces to keep their native spatial shapes with desired levels of flexibility or rigidity. As a mesoscopic soft-potential simulation technique MFD exhibits attractive features like a comparatively simple setup of start geometries (not being particularly prone to molecular entanglements or caging effects) and comparatively short simulation times for simulations on the microseconds scale for molecular ensembles representing millions of atoms. In summary MFD may become an interesting simulation alternative for biomolecular research and development which enriches the set of already available and proven techniques, especially for the study of interactions between proteins and molecular superstructures like membranes or artificial molecular layers with technical relevance as well as protein−protein interactions. After extended application to additional fields of research a more thorough method comparison of the new MFD extension with alternative molecular simulation techniques regarding their specific strengths and weaknesses will become possible to then allow a validated and useful assessment.

AUTHOR INFORMATION

Corresponding Author

*E-mail: andreas.truszkowski@w-hs.de.

Notes

The authors declare no competing financial interest.

ACKNOWLEDGMENTS

The authors would like to thank the reviewers for corrections and helpful suggestions.

REFERENCES

(1) Singer, S. J.; Nicolson, G. L. The Fluid Mosaic Model of the Structure of Cell Membranes. *Science* **1972**, *175*, 720−731.
(2) Chernomordik, L. V.; Kozlov, M. M. Mechanics of Membrane Fusion. *Nat. Struct. Mol. Biol.* **2008**, *15*, 675−683.
(3) Lipowsky, R. The Conformation of Membranes. *Nature* **1991**, *349*, 475−481.
(4) Berg, J. M., Tymoczko, J. L., Stryer, L. *Biochemistry*, 6th ed.; Elsevier GmbH: München, 2007; p 1224.
(5) van Meer, G. Lipid Traffic in Animal Cells. *Annu. Rev. Cell Biol.* **1989**, *5*, 247−275.
(6) van Meer, G.; Voelker, D. R.; Feigenson, G. W. Membrane Lipids: Where They are and how They Behave. *Nat. Rev. Mol. Cell Biol.* **2008**, *9*, 112−124.
(7) Zachowski, A. Phospholipids in Animal Eukaryotic Membranes: Transverse Asymmetry and Movement. *Biochem. J.* **1993**, *294*, 1−14.
(8) Dowhan, W. Molecular Basis For Membrane Phospholipid Diversity: Why Are There So Many Lipids? *Annu. Rev. Biochem.* **1997**, *66*, 199−232.
(9) Beierlein, F.; Lanig, H.; Schürer, G.; Horn, A. H. C.; Clark, T. Quantum Mechanical/molecular Mechanical (QM/MM) Docking: An Evaluation for Known Test Systems. *Mol. Phys.* **2003**, *101*, 2469−2480.
(10) van der Kamp, M. W.; Mulholland, A. J. Combined Quantum Mechanics/Molecular Mechanics (QM/MM) Methods in Computational Enzymology. *Biochemistry* **2013**, *52*, 2708−2728.
(11) Lin, H.; Truhlar, D. G. QM/MM: What Have we Learned, Where are we, and Where do we go From Here? *Theor. Chem. Acc.* **2006**, *117*, 185−199.
(12) Groenhof, G. Solving Chemical Problems With a Mixture of Quantum-mechanical and Molecular Mechanics Calculations: Nobel Prize in Chemistry 2013. *Angew. Chem., Int. Ed. Engl.* **2013**, *52*, 12489−12491.
(13) Ng, H.; Laughton, C.; Doughty, S. Molecular Dynamics Simulations of the Adenosine A2a Receptor in POPC and POPE Lipid Bilayers: Effects of Membrane on Protein Behavior. *J. Chem. Inf. Model.* **2014**, *54*, 573−581.
(14) Martinez-Archundia, M.; Cordomi, A.; Garriga, P.; Perez, J. J. Molecular Modeling of the M3 Acetylcholine Muscarinic Receptor and Its Binding Site. *J. Biomed Biotechnol* **2012**, *2012*, 1−12.
(15) Feller, S. E.; Venable, R. M.; Pastor, R. W. Computer Simulation of a DPPC Phospholipid Bilayer: Structural Changes as a Function of Molecular Surface Area. *Langmuir* **1997**, *13*, 6555−6561.
(16) Shaw, D. E.; Maragakis, P.; Lindorff-Larsen, K.; Piana, S.; Dror, R. O.; Eastwood, M. P.; Bank, J. A.; Jumper, J. M.; Salmon, J. K.; Shan, Y.; Wriggers, W. Atomic-level Characterization of the Structural Dynamics of Proteins. *Science* **2010**, *330*, 341−346.
(17) Shaw, D.; Dror, R. Millisecond-scale Molecular Dynamics Simulations on Anton. *High Performance Computing Networking, Storage and Analysis* **2009**, 1−11.
(18) Gunsteren, W.; Berendsen, H.; Geurtsen, R.; Zwinderman, H. A Molecular Dynamics Computer Simulation of an Eight-Base-Pair DNA Fragment in Aqueous Solution: Comparison With Experimental Two-Dimensional NMR. *Ann. N.Y. Acad. Sci.* **1986**, *482*, 287−303.
(19) Durrant, J. D.; McCammon, J. A. Molecular Dynamics Simulations and Drug Discovery. *BMC Biol.* **2011**, DOI: 10.1186/1741-7007-9-71.
(20) Monticelli, L.; Kandasamy, S. K.; Periole, X.; Larson, R. G.; Tieleman, D. P.; Marrink, S.-J. The MARTINI Coarse-Grained Force Field: Extension to Proteins. *J. Chem. Theory Comput.* **2008**, *4*, 819−834.
(21) Shillcock, J. C.; Lipowsky, R. Equilibrium Structure and Lateral Stress Distribution of Amphiphilic Bilayers From Dissipative Particle Dynamics Simulations. *J. Chem. Phys.* **2002**, *117*, 5048−5061.
(22) Scott, K. a.; Bond, P. J.; Ivetac, A.; Chetwynd, A. P.; Khalid, S.; Sansom, M. S. P. Coarse-grained MD Simulations of Membrane Protein-bilayer Self-assembly. *Structure* **2008**, *16*, 621−630.
(23) Piñeiro, A.; Bond, P. J.; Khalid, S. Exploring the Conformational Dynamics and Membrane Interactions of PorB From C. Glutamicum: A Multi-scale Molecular Dynamics Simulation Study. *Biochim. Biophys. Acta, Biomembr.* **2011**, *1808*, 1746−1752.
(24) Yamamoto, S.; Maruyama, Y.; Hyodo, S.-a. Dissipative Particle Dynamics Study of Spontaneous Vesicle Formation of Amphiphilic Molecules. *J. Chem. Phys.* **2002**, *116*, 5842.
(25) Marrink, S. J.; Mark, A. E. The Mechanism of Vesicle Fusion as Revealed by Molecular Dynamics Simulations. *J. Am. Chem. Soc.* **2003**, *125*, 11144−11145.
(26) Marrink, S. J.; Lindahl, E.; Edholm, O.; Mark, a. E. Simulation of the Spontaneous Aggregation of Phospholipids Into Bilayers. *J. Am. Chem. Soc.* **2001**, *123*, 8638−8639.
(27) Marrink, S. J.; Risselada, H. J.; Yefimov, S.; Tieleman, D. P.; de Vries, A. H. The MARTINI Force Field: Coarse Grained Model for Biomolecular Simulations. *J. Phys. Chem. B* **2007**, *111*, 7812−7824.

DOI: 10.1021/ci5006096
J. Chem. Inf. Model. 2015, 55, 983−997

(28) Li, D.-W.; Liu, X. Y. Examination of Membrane Fusion by Dissipative Particle Dynamics Simulation and Comparison With Continuum Elastic Models. *J. Chem. Phys.* **2005**, *122*, 174909.
(29) Kranenburg, M.; Venturoli, M.; Smit, B. Phase Behavior and Induced Interdigitation in Bilayers Studied With Dissipative Particle Dynamics. *J. Phys. Chem. A* **2003**, *107*, 11491−11501.
(30) Knecht, V.; Marrink, S.-J. Molecular Dynamics Simulations of Lipid Vesicle Fusion in Atomic Detail. *Biophys. J.* **2007**, *92*, 4254−4261.
(31) Knecht, V.; Mark, A. E.; Marrink, S.-J. Phase Behavior of a Phospholipid/fatty Acid/water Mixture Studied in Atomic Detail. *J. Am. Chem. Soc.* **2006**, *128*, 2030−2034.
(32) Illya, G.; Lipowsky, R.; Shillcock, J. C. Two-component Membrane Material Properties and Domain Formation From Dissipative Particle Dynamics. *J. Chem. Phys.* **2006**, *125*, 114710.
(33) Grafmüller, A.; Shillcock, J.; Lipowsky, R. The Fusion of Membranes and Vesicles: Pathway and Energy Barriers From Dissipative Particle Dynamics. *Biophys. J.* **2009**, *96*, 2658−2675.
(34) Goetz, R.; Lipowsky, R. Computer Simulations of Bilayer Membranes: Self-assembly and Interfacial Tension. *J. Chem. Phys.* **1998**, *108*, 7397−7409.
(35) Goetz, R.; Gompper, G.; Lipowsky, R. Mobility and Elasticity of Self-assembled Membranes. *Phys. Rev. Lett.* **1999**, *82*, 221−224.
(36) Gao, L.; Shillcock, J.; Lipowsky, R. Improved Dissipative Particle Dynamics Simulations of Lipid Bilayers. *J. Chem. Phys.* **2007**, *126*, 015101.
(37) Castillo, N.; Monticelli, L.; Barnoud, J.; Tieleman, D. P. Free Energy of WALP23 Dimer Association in DMPC, DPPC, and DOPC Bilayers. *Chem. Phys. Lipids* **2013**, 1−11.
(38) Muller, M.; Katsov, K.; Schick, M. New Mechanism of Membrane Fusion. *J. Chem. Phys.* **2002**, *116*, 2342−2345.
(39) Groot, R. D. Electrostatic Interactions in Dissipative Particle Dynamics-simulation of Polyelectrolytes and Anionic Surfactants. *J. Chem. Phys.* **2003**, *118*, 11265−11277.
(40) Hoogerbrugge, P.; Koelman, J. Simulating Microscopic Hydrodynamic Phenomena With Dissipative Particle Dynamics. *Europhys. Lett.* **1992**, *19*, 155−160.
(41) Koelman, J.; Hoogerbrugge, P. Dynamic Simulations of Hard-sphere Suspensions Under Steady Shear. *Europhys. Lett.* **1993**, *21*, 363−368.
(42) Guo, X. D.; Zhang, L. J.; Wu, Z. M.; Qian, Y. Dissipative Particle Dynamics Studies on Microstructure of PH-Sensitive Micelles for Sustained Drug Delivery. *Macromolecules* **2010**, *43*, 7839−7844.
(43) Truszkowski, A.; Epple, M.; Fiethen, A.; Zielesny, A.; Kuhn, H. Molecular Fragment Dynamics Study on the Water-air Interface Behavior of Non-ionic Polyoxyethylene Alkyl Ether Surfactants. *J. Colloid Interface Sci.* **2013**, *410*, 140−145.
(44) Schulz, S. G.; Kuhn, H.; Schmid, G.; Mund, C.; Venzmer, J. Phase Behavior of Amphiphilic Polymers: A Dissipative Particles Dynamics Study. *Colloid Polym. Sci.* **2004**, *283*, 284−290.
(45) Ryjkina, E.; Kuhn, H.; Rehage, H.; Müller, F.; Peggau, J. Molecular Dynamic Computer Simulations of Phase Behavior of Non-ionic Surfactants. *Angew. Chem., Int. Ed.* **2002**, *41*, 983−986.
(46) Espanol, P. Hydrodynamics From Dissipative Particle Dynamics. *Phys. Rev. A* **1995**, *52*, 1734−1742.
(47) Warren, P. B. Dissipative Particle Dynamics. *Curr. Opin. Colloid Interface Sci.* **1998**, *3*, 620−624.
(48) Flekkoy, E. G.; Coveney, P. V. From Molecular Dynamics to Dissipative Particle Dynamics. *Phys. Rev. Lett.* **1999**, *83*, 1775−1778.
(49) Verlet, L. Computer "experiments" on Classical Fluids. I. Thermodynamical Properties of Lennard-Jones Molecules. *Phys. Rev. A* **1967**, 159−165.
(50) Swope, W. C. A Computer Simulation Method for the Calculation of Equilibrium Constants for the Formation of Physical Clusters of Molecules: Application to Small Water Clusters. *J. Chem. Phys.* **1982**, *76*, 637−649.
(51) Espanol, P.; Warren, P. Statistical Mechanics of Dissipative Particle Dynamics. *Europhys. Lett.* **1995**, *30*, 191−196.
(52) Pagonabarraga, I. Self-consistent Dissipative Particle Dynamics Algorithm. *Europhys. Lett.* **1998**, *42*, 377−382.
(53) Pagonabarraga, I.; Frenkel, D. Dissipative Particle Dynamics for Interacting Systems. *J. Chem. Phys.* **2001**, *115*, 5015−5027.
(54) Frenkel, D., Smit, B. *Understanding Molecular Simulation: From Algorithms to Applications*; Academic Press, 2002; p 638.
(55) Groot, R. D.; Warren, P. B. Dissipative Particle Dynamics: Bridging the gap Between Atomistic and Mesoscopic Simulation. *J. Chem. Phys.* **1997**, *107*, 4423−4435.
(56) Brini, E.; Algaer, E. a.; Ganguly, P.; Li, C.; Rodríguez-Ropero, F.; van der Vegt, N. F. a. Systematic Coarse-graining Methods for Soft Matter Simulations - a Review. *Soft Matter* **2013**, *9*, 2108−2119.
(57) Schulz, S.; Kuhn, H.; Schmid, G. Molecular Modeling Computer Simulations of Organic Polymers: A Novel Computer Simulation Technique to Characterize Nanostructured Materials. *MRS Proc.* **2004**, DOI: 10.1557/proc-788-l10.5.
(58) Sun, H. COMPASS: An ab Initio Force-Field Optimized for Condensed-Phase ApplicationsOverview With Details on Alkane and Benzene Compounds. *J. Phys. Chem. A* **1998**, *102*, 7338−7364.
(59) González-Melchor, M.; Mayoral, E.; Velázquez, M. E.; Alejandre, J. Electrostatic Interactions in Dissipative Particle Dynamics Using the Ewald Sums. *J. Chem. Phys.* **2006**, *125*, 224107.
(60) Ibergay, C.; Malfreyt, P.; Tildesley, D. J. Electrostatic Interactions in Dissipative Particle Dynamics: Toward a Mesoscale Modeling of the Polyelectrolyte Brushes. *J. Chem. Theory Comput.* **2009**, *5*, 3245−3259.
(61) Truszkowski, A.; Daniel, M.; Kuhn, H.; Neumann, S.; Steinbeck, C.; Zielesny, A.; Epple, M. A Molecular Fragment Cheminformatics Roadmap for Mesoscopic Simulation. *J. Cheminf.* **2014**, *6*, 45.
(62) Berman, H. M.; Westbrook, J.; Feng, Z.; Gilliland, G.; Bhat, T. N.; Weissig, H.; Shindyalov, I. N.; Bourne, P. E. The Protein Data Bank. *Nucleic Acids Res.* **2000**, *28*, 235−242.
(63) Wang, X. Solution Structure of Decorin-binding Protein A From Borrelia Burgdorferi. *Biochemistry* **2012**, *51*, 8353−8362.
(64) MFD-FormulaOne, pre-release, version 1.1.0.0. MFD-FormulaOne is a product of CAM-D Technologies GmbH (www.molecular-dynamics.de) and GNWI-Gesellschaft fuer naturwissenschaftliche Informatik mbH (www.gnwi.de); http://www.mfd-formulaOne.de (accessed December 13, 2014).
(65) CAM-D Technologies GmbH. http://www.molecular-dynamics.de/ (accessed January 21, 2015).
(66) Schulz, S. G.; Frieske, U.; Kuhn, H.; Schmid, G.; Muller, F.; Mund, C.; Venzmer, J. Mesoscale Computer Simulations on the Phase Behavior of the Non-ionic Surfactant C12E5. *Tenside, Surfactants, Deterg.* **2004**, *41*, 230−234.
(67) Kiselev, M. A.; Zemlyanaya, E. V.; Aswal, V. K.; Neubert, R. H. H. What can we Learn About the Lipid Vesicle Structure From the Small-angle Neutron Scattering Experiment? *Eur. Biophys. J.* **2006**, *35*, 477−93.
(68) Lewis, B. a.; Engelman, D. M. Lipid Bilayer Thickness Varies Linearly With Acyl Chain Length in Fluid Phosphatidylcholine Vesicles. *J. Mol. Biol.* **1983**, *166*, 211−217.
(69) Andersen, O. S.; Koeppe, R. E. Bilayer Thickness and Membrane Protein Function: An Energetic Perspective. *Annu. Rev. Biophys. Biomol. Struct.* **2007**, *36*, 107−310.
(70) Bermúdez, H.; Hammer, D. a.; Discher, D. E. Effect of Bilayer Thickness on Membrane Bending Rigidity. *Langmuir* **2004**, *20*, 540−543.
(71) Edidin, M. Lipids on the Frontier: A Century of Cell-membrane Bilayers. *Nat. Rev. Mol. Cell Biol.* **2003**, *4*, 414−418.
(72) Fujiki, Y.; Hubbard, a. L.; Fowler, S.; Lazarow, P. B. Isolation of Intracellular Membranes by Means of Sodium Carbonate Treatment: Application to Endoplasmic Reticulum. *J. Cell Biol.* **1982**, *93*, 97−102.
(73) Larsson, K. On Periodic Curvature and Standing Wave Motions in Cell Membranes. *Chem. Phys. Lipids* **1997**, *88*, 15−20.
(74) Wimley, W. C.; Thompson, T. E. Exchange and Flip-flop of Dimyristoylphosphatidylcholine in Liquid-crystalline, Gel, and Two-component, Two-phase Large Unilamellar Vesicles. *Biochemistry* **1990**, *29*, 1296−1303.

DOI: 10.1021/ci5006096
J. Chem. Inf. Model. 2015, 55, 983−997

(75) Brown, K. L.; Conboy, J. C. Lipid Flip-flop in Binary Membranes Composed of Phosphatidylserine and Phosphatidylcholine. *J. Phys. Chem. A* **2013**, *117*, 15041−15050.
(76) Gurtovenko, A. A.; Vattulainen, I. Molecular Mechanism for Lipid Flip-flops. *J. Phys. Chem. B* **2007**, *111*, 13554−13559.
(77) Gerelli, Y.; Porcar, L.; Lombardi, L.; Fragneto, G. Lipid Exchange and Flip-flop in Solid Supported Bilayers. *Langmuir* **2013**, *29*, 12762−9.
(78) Kumar, V. V. Complementary Molecular Shapes and Additivity of the Packing Parameter of Lipids. *Proc. Natl. Acad. Sci. U. S. A.* **1991**, *88*, 444−448.
(79) Winter, R., Noll, F. *Methoden der Biophysikalischen Chemie*; Vieweg+Teubner Verlag: Stuttgart, 2011; p 576.
(80) Baumgärtner, P.; Geiger, M.; Zieseniss, S.; Malleier, J.; Huntington, J. a.; Hochrainer, K.; Bielek, E.; Stoeckelhuber, M.; Lauber, K.; Scherfeld, D.; Schwille, P.; Wäldele, K.; Beyer, K.; Engelmann, B. Phosphatidylethanolamine Critically Supports Internalization of Cell-penetrating Protein C Inhibitor. *J. Cell Biol.* **2007**, *179*, 793−804.
(81) Korlach, J.; Schwille, P.; Webb, W. W.; Feigenson, G. W. Characterization of Lipid Bilayer Phases by Confocal Microscopy and Fluorescence Correlation Spectroscopy. *Proc. Natl. Acad. Sci. U. S. A.* **1999**, *96*, 8461−8466.
(82) Haluska, C. K.; Riske, K. A.; Lehn, J.-M.; Lipowsky, R.; Dimova, R. Time Scales of Membrane Fusion Revealed by Direct Imaging of Vesicle Fusion With High. *Proc. Natl. Acad. Sci. U.S.A.* **2006**, *103*, 15841−15846.
(83) Lindau, M.; Alvarez de Toledo, G. The Fusion Pore. *Biochim. Biophys. Acta, Mol. Cell Res.* **2003**, *1641*, 167−173.
(84) Kursula, P. Crystallographic Snapshots of Initial Steps in the Collapse of the Calmodulin Central Helix. *Acta Crystallogr. D Biol. Crystallogr.* **2014**, *70*, 24−30.
(85) Seaton, B. a.; Head, J. F.; Engelman, D. M.; Richards, F. M. Calcium-induced Increase in the Radius of Gyration and Maximum Dimension of Calmodulin Measured by Small-angle X-ray Scattering. *Biochemistry* **1985**, *24*, 6740−6743.
(86) Fermi, G.; Perutz, M. F.; Shaanan, B.; Fourme, R. The Crystal Structure of Human Deoxyhaemoglobin at 1.74 A Resolution. *J. Mol. Biol.* **1984**, *175*, 159−174.
(87) Vandegriff, K. D.; McCarthy, M.; Rohlfs, R. J.; Winslow, R. M. Colloid Osmotic Properties of Modified Hemoglobins: Chemically Cross-linked Versus Polyethylene Glycol Surface-conjugated. *Biophys. Chem.* **1997**, *69*, 23−30.
(88) Daly, N. L.; Rosengren, K. J.; Craik, D. J. Discovery, Structure and Biological Activities of Cyclotides. *Adv. Drug Delivery Rev.* **2009**, *61*, 918−930.
(89) Barry, D. G.; Daly, N. L.; Clark, R. J.; Sando, L.; Craik, D. J. Linearization of a Naturally Occurring Circular Protein Maintains Structure but Eliminates Hemolytic Activity. *Biochemistry* **2003**, *42*, 6688−6695.
(90) Herrmann, A.; Svangård, E.; Claeson, P.; Gullbo, J.; Bohlin, L.; Göransson, U. Key Role of Glutamic Acid for the Cytotoxic Activity of the Cyclotide Cycloviolacin O2. *CMLS Cell Mol. Life Sci.* **2006**, *63*, 235−45.
(91) Svangård, E.; Burman, R.; Gunasekera, S.; Lövborg, H.; Gullbo, J.; Göransson, U. Mechanism of Action of Cytotoxic Cyclotides: Cycloviolacin O2 Disrupts Lipid Membranes. *J. Nat. Prod.* **2007**, *70*, 643−647.
(92) Rosengren, K. J.; Daly, N. L.; Plan, M. R.; Waine, C.; Craik, D. J. Twists, Knots, and Rings in Proteins. Structural Definition of the Cyclotide Framework. *J. Biol. Chem.* **2003**, *278*, 8606−8616.
(93) Henriques, S. T.; Huang, Y.-H.; Castanho, M. A. R. B.; Bagatolli, L. A.; Sonza, S.; Tachedjian, G.; Daly, N. L.; Craik, D. J. Phosphatidylethanolamine Binding is a Conserved Feature of Cyclotide-membrane Interactions. *J. Biol. Chem.* **2012**, *287*, 33629−33643.
(94) Shenkarev, Z. O.; Nadezhdin, K. D.; Sobol, V. A.; Sobol, A. G.; Skjeldal, L.; Arseniev, A. S. Conformation and Mode of Membrane Interaction in Cyclotides. Spatial Structure of Kalata B1 Bound to a Dodecylphosphocholine Micelle. *FEBS J.* **2006**, *273*, 2658−2672.
(95) Burman, R.; Gunasekera, S.; Strömstedt, A. a.; Göransson, U. Chemistry and Biology of Cyclotides: Circular Plant Peptides Outside the Box. *J. Nat. Prod.* **2014**, *77*, 724−736.
(96) Gründemann, C.; Thell, K.; Lengen, K.; Garcia-Käufer, M.; Huang, Y.-H.; Huber, R.; Craik, D. J.; Schabbauer, G.; Gruber, C. W. Cyclotides Suppress Human T-Lymphocyte Proliferation by an Interleukin 2-Dependent Mechanism. *PLoS One* **2013**, *8*, e68016.
(97) Huang, Y.-H.; Colgrave, M. L.; Daly, N. L.; Keleshian, A.; Martinac, B.; Craik, D. J. The Biological Activity of the Prototypic Cyclotide Kalata b1 is Modulated by the Formation of Multimeric Pores. *J. Biol. Chem.* **2009**, *284*, 20699−707.
(98) Wang, C. K.; Wacklin, H. P.; Craik, D. J. Cyclotides Insert Into Lipid Bilayers to Form Membrane Pores and Destabilize the Membrane Through Hydrophobic and Phosphoethanolamine-specific Interactions. *J. Biol. Chem.* **2012**, *287*, 43884−43898.
(99) Nawae, W.; Hannongbua, S.; Ruengjitchatchawalya, M. Defining the Membrane Disruption Mechanism of Kalata B1 via Coarse-grained Molecular Dynamics Simulations. *Sci. Rep.* **2014**, *4*, 1−9.

DOI: 10.1021/ci5006096
J. Chem. Inf. Model. 2015, 55, 983−997